

SIMULATION OF TSUNAMI ACCOMPANIED BY BREAKING SHORT-PERIOD WAVES

Takashi Tomita¹ and Kenya Takahashi²

The 2011 Tohoku tsunami hitting Kuji port, Japan, was high whose height of 5.4 m was measured in the water area of 49.5 m deep in front of the open mouth of the port. This tsunami was accompanied by short-period waves while it propagated in the port, and then it broke in the port of 18 m deep approximately ahead on a breakwater. Since wave pressure by a tsunami with short-period waves is important for design of breakwaters according to Ikeno et al. (2006), such wave transformation and deformation should be able to be calculated for planning and designing measures to save people and reduce property loss. In this study, a non-hydrostatic mathematical model was developed to calculate tsunamis including short period waves, and validated in comparison with experimental results in which the tsunami in Kuji port was modeled.

Keywords: Tsunami; undular bore; numerical simulation; wave breaking model; non-hydrostatic model

INTRODUCTION

The 2011 off the Pacific coast of Tohoku earthquake with moment magnitude (Mw) 9.0 triggered a catastrophic tsunami mainly hitting Tohoku and Kanto regions in Japan. The 40 m runup heights of the tsunami were measured in Ryori and Taro of Iwate prefecture in the Sanriku coast. The tsunami also hit Kuji port, which is the most north port in Iwate prefecture and located in the northern part of the Sanriku coast. The water area of Kuji port occupies almost all of the Kuji bay. Height of tsunami traces along the coast of Kuji port ranged from 6 m to 16 m, resulting in the 3.7 km² area inundated and two persons dead and two missing.

The tsunami hitting Kuji port was an undular bore which was a type of tsunami that had a steep front and was accompanied by short-period waves, as shown in Figure 1. As shown in the figure, the undular bore broke in front of a breakwater installed in the innermost of the bay and the broken undular bore hit the breakwater, which was little damaged. The tsunami overtopping the breakwater and diffracted by the breakwater formed the undular bore again behind the breakwater, and hit the coast dynamically. According to Ikeno et al. (2006), wave pressure of an undular bore acting on a vertical wall is 1.36 times as strong as a normal tsunami without short-period waves. The undular bore, therefore, is of importance to coastal defense facilities against tsunamis. So far undular bores could be recognized, for example, in rivers such as the tsunami by the 2013 off Tokachi earthquake (PIANC 2010) and on mild slope beaches such as the tsunami by the 1983 off Nihon-kai Chubu earthquake (Shuto 2007).



Figure 1. Snapshots from a video footage of the 2011 Tohoku tsunami hitting Kuji port, taken by Kamaishi Port Office, Tohoku Regional Development Bureau of Ministry of Land, infrastructure, Transport and Tourism, Japan.

Experimental and numerical investigation by Kubota et al. (1986) has indicated that tsunami wave slope $(H/T(gh))^{-1/2}$ in which H is the wave height, T wave period h water depth, and g gravitational acceleration) to generate undular bores is over 1.25×10^{-4} in the case of bottom slope = 1/200, and over 3.76×10^{-4} in the case of bottom slope = 1/100. This means that possibility that a normal tsunami is transformed to an undular bore depending on wave height and period of a tsunami as well as the bottom slope angle. If a tsunami is high, it may be transformed to an undular bore even in a deep water

¹ Marine Information and Tsunami Division, Port and Airport Research Institute, 3-1-1 Nagase, Yokosuka, Kanagawa 239-0826, Japan

² Penta-Ocean Construction Co. Ltd., 2-2-8 Koraku, Bunkyo-ku, Tokyo 112-8576, Japan

area. Indeed, the 2011 Tohoku tsunami propagating to Kuji port was measured by a pressure gauge on a directional wave meter mounted on the seabed of 49.5 m deep in front of the open mouth of the port. The peak sea surface elevation of the tsunami was 5.4 m, as shown in Figure 2. Since the measuring instrument was broken 35 seconds after measuring the peak value, the peak value may not be the maximum value of the first wave of the tsunami. However, the front slope of the first tsunami wave is as steep as the peak value appears within 1 minute from the mean water level.

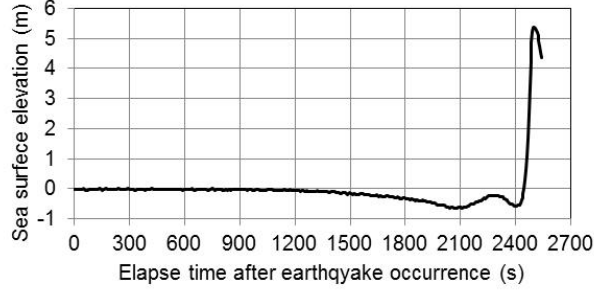


Figure 2. Tsunami waveform measured in front of the open mouth of Kuji port whose depth is 49.5m.

To calculate undular bores, we can no longer use the conventional tsunami simulation model based on the nonlinear long wave theory, because the theory uses the assumption of hydrostatic pressure whereas the undular bore was wave transformation in the non-hydrostatic pressure field. Therefore, we have used models for dispersive waves such as Boussinesq models (Madsen and Sørensen 1993, Nwogu 1993). In order to understand and predict a high tsunami such as the maximum considered tsunami, authors have developed a three-dimensional non-hydrostatic mathematical simulation model of tsunamis to calculate wave transformation and deformation of a tsunami (Tomita et al. 2007, Honda and Tomita 2009). In this study, the tsunami simulation model was validated in comparison with experimental results to model the tsunami in Kuji port. Since the original tsunami simulation model had no wave breaking model, the wave breaking model by Kennedy et al. (2000) with coefficients by Lynett (2006) was introduced in the tsunami simulation model in this study.

MATHEMATICAL MODEL

Governing Equations

For calculation of an undular bore in this study, a sub-model, STOC-IC, in the Storm Surge and Tsunami Simulator in Coastal Areas and Oceans (STOC) (Tomita et al. 2007) was used. STOC-IC is based on the Navier-Stokes equations with the SGS turbulent model and continuity equation, as described by

$$\begin{aligned} & \gamma_v \frac{\partial u}{\partial t} + \frac{\partial}{\partial x}(\gamma_x uu) + \frac{\partial}{\partial y}(\gamma_y vu) + \frac{\partial}{\partial z}(\gamma_z wu) - f_0 v \\ & = -\gamma_v \frac{1}{\rho} \frac{\partial p}{\partial x} + \frac{\partial}{\partial x} \left(\gamma_x \nu_e 2 \frac{\partial u}{\partial x} \right) + \frac{\partial}{\partial y} \left\{ \gamma_y \nu_e \left(\frac{\partial u}{\partial y} + \frac{\partial v}{\partial x} \right) \right\} + \frac{\partial}{\partial z} \left\{ \gamma_z \nu_e \left(\frac{\partial u}{\partial z} + \frac{\partial w}{\partial x} \right) \right\} \end{aligned} \quad (1)$$

$$\begin{aligned} & \gamma_v \frac{\partial v}{\partial t} + \frac{\partial}{\partial x}(\gamma_x uv) + \frac{\partial}{\partial y}(\gamma_y vv) + \frac{\partial}{\partial z}(\gamma_z wv) + f_0 u \\ & = -\gamma_v \frac{1}{\rho} \frac{\partial p}{\partial y} + \frac{\partial}{\partial x} \left\{ \gamma_x \nu_e \left(\frac{\partial v}{\partial x} + \frac{\partial u}{\partial y} \right) \right\} + \frac{\partial}{\partial y} \left(\gamma_y \nu_e 2 \frac{\partial v}{\partial y} \right) + \frac{\partial}{\partial z} \left\{ \gamma_z \nu_e \left(\frac{\partial v}{\partial z} + \frac{\partial w}{\partial y} \right) \right\} \end{aligned} \quad (2)$$

$$\begin{aligned} & \gamma_v \frac{\partial w}{\partial t} + \frac{\partial}{\partial x}(\gamma_x uw) + \frac{\partial}{\partial y}(\gamma_y vw) + \frac{\partial}{\partial z}(\gamma_z ww) \\ & = -\gamma_v g - \gamma_v \frac{1}{\rho} \frac{\partial p}{\partial z} + \frac{\partial}{\partial x} \left\{ \gamma_x \nu_e \left(\frac{\partial w}{\partial x} + \frac{\partial u}{\partial z} \right) \right\} + \frac{\partial}{\partial y} \left\{ \gamma_y \nu_e \left(\frac{\partial w}{\partial y} + \frac{\partial v}{\partial z} \right) \right\} + \frac{\partial}{\partial z} \left(\gamma_z \nu_e 2 \frac{\partial w}{\partial z} \right) \end{aligned} \quad (3)$$

$$\frac{\partial}{\partial x}(\gamma_x u) + \frac{\partial}{\partial y}(\gamma_y v) + \frac{\partial}{\partial z}(\gamma_z w) = 0 \quad (4)$$

$$\nu_e = (C_s \Delta)^2 \sqrt{S_{ij} S_{ij}}, \quad S_{ij} = \left(\frac{\partial u_i}{\partial x_j} + \frac{\partial u_j}{\partial x_i} \right), \quad \Delta = \sqrt[3]{\Delta x \Delta y \Delta z} \quad (5), (6), (7)$$

in which x , y and z are the Cartesian coordinates, u , v and w the velocity in the directions of x , y and z respectively, ρ the fluid density, p the pressure, g the gravitational acceleration, ν_e the eddy viscosity, f_0 the Coriolis coefficient, Δx , Δy and Δz the computational grid space in the directions of x , y and z , respectively, and C_s the coefficient for the Smagorinsky-type turbulent model, which is 0.2 (Fujima et al. 2002, Honda and Tomita 2008). The porosity of γ_x in each computation cell and transmissivity of γ_x , γ_y or γ_z in each cell surface perpendicular to the x , y or z direction (Sakakiyama and Kajima 1992) are introduced in the momentum and continuity equations in order to treat configurations of the sea bottom and shapes of structures smoothly in a computation field. Since no assumption is applied in pressure calculation, STOC-IC is capable of calculating undular bores.

Wave Breaking Model

The free water surface is detected by the integrated continuity equation in a similar way of the conventional model of tsunami propagation and inundation which is based on the non-linear long wave theory described by the depth-integrated equations. Therefore, for calculation of wave breaking of an undular bore, the wave breaking model by Kennedy et al. (2000) is installed into STOC-IC. Kennedy's wave breaking model has been developed as an eddy viscosity-type model for Boussinesq equations. The parameters of this wave breaking model have been modified by Lynett (2006) in order to apply it to a two-layer fluid model. In this study, this modified wave breaking model is introduced in STOC-IC.

Numerical Scheme

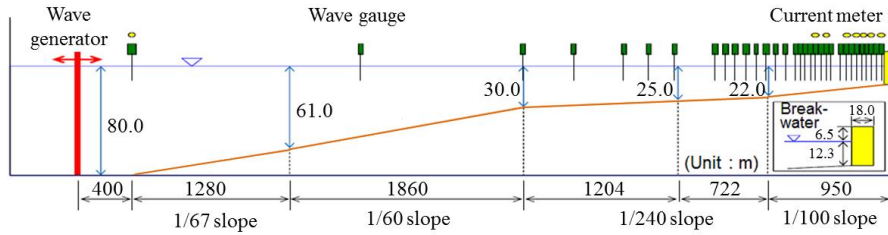
The governing equations shown in Equations of (1) to (7) were discretized using the finite difference technique on staggered grids. The pressure, free surface elevation and viscosity were located at the computational cell center, while velocity components were set at the cell faces. Setting the different control volume for different physical quantities in the staggered grid system, the simplified maker and cell (SMAC) method was applied to solve the momentum and continuity equations. Spatial difference was discretized by the first-order upwind difference scheme except for advection terms which were discretized by a hybrid scheme of the upwind difference and second-order central difference. For example, using the weighting parameter α , the second term in the left hand side of Eq. (1) was given by

$$\frac{\partial \gamma_x u u}{\partial x} = \begin{cases} \frac{1}{\Delta x} \left[\alpha (\gamma_{xi} u_i u_i - \gamma_{xi-1} u_{i-1} u_{i-1}) + (1 - \alpha) \frac{(\gamma_{xi+1} u_{i+1} u_{i+1} - \gamma_{xi-1} u_{i-1} u_{i-1})}{2} \right], & u_i \geq 0 \\ \frac{1}{\Delta x} \left[\alpha (\gamma_{xi+1} u_{i+1} u_{i+1} - \gamma_{xi} u_i u_i) + (1 - \alpha) \frac{(\gamma_{xi+1} u_{i+1} u_{i+1} - \gamma_{xi-1} u_{i-1} u_{i-1})}{2} \right], & u_i < 0 \end{cases} \quad (5)$$

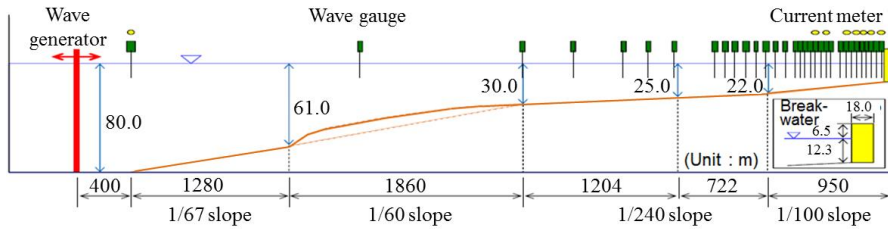
Preliminary investigation showed that the calculation result of $\alpha=0.2$ was in good agreement with an experimental result of a tsunami propagating over a wide-crown trapezium in the case of that Δx was 1/25 times or less of the wavelength and Δz was 2.0 times or less of the tsunami height.

OUTLINE OF MODEL EXPERIMENT

Kashima and Hirayama (2013) have carried out a series of model experiments in a wave flume of 35 m long, as shown in Figure 3. In the wave flume is constructed two types models based on the seabed profile of Kuji port from the front of the breakwater where the water depth is 12.3 m to the offshore point about 6 km off the breakwater where the water depth is 80 m. The model scale is 1/200. The wave profiles are measured by electric-capacitance-type wave gauges, and fluid velocities in the wave propagation direction are measured by propeller-type current meters. The incident waves in the experiment are based on the waveform until when the maximum value appeared in the first tsunami which is calculated in a tsunami propagation simulation to reproduce the waveform measured by a GPS-mounted buoy installed off the open mouth of Kuji bay where the water depth is 125 m. Table 1 indicates conditions of the experimental incident waves in the scale of the field. Five solitary waves corresponding to the incident wave conditions are generated by a piston-type wave generator.



(1) Configuration of bottom without a hump



(b) Configuration of bottom with a hump

Figure 3. Experimental setup in the scale of the field.

Table 1. Incident wave condition in the scale of the field.

Case	T_{in} (s)	H_{in} (m)
1	67.9	4.0
2	67.9	5.0
3	110.3	4.0
4	110.3	5.0
5	110.3	6.0

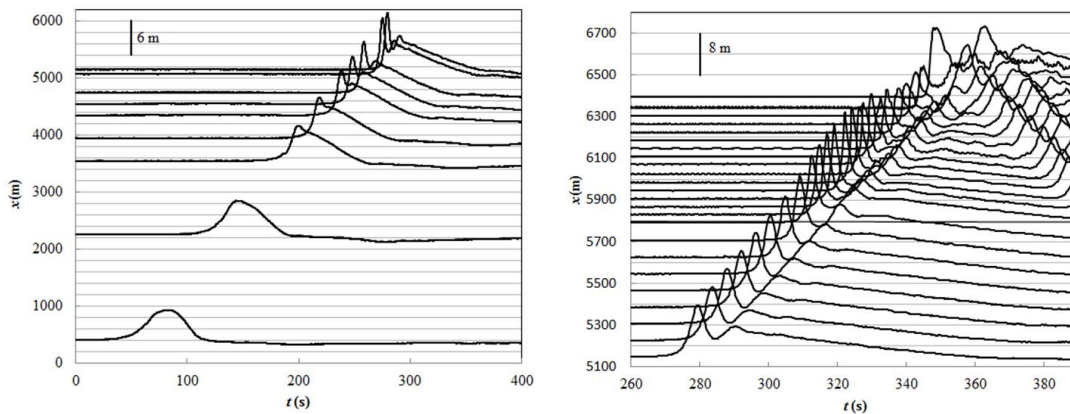


Figure 4. Time waveforms in Case 2 on the bottom with the hump.

Figure 4 indicates time waveforms measured at all positions in the experiment of Case 2 on the bottom profile with the hump, in which x is the distance from the wave maker and graphical scales are indicated for measuring the waveforms. The left figure indicates the waveforms before the position of $x=5146$ m, which is 320 m ahead of the tip of the fourth slope of 1/100, while the right indicates those behind the position of $x=5146$ m. The waveform at the tip of the first slope of 1/67 is almost symmetrical, while the water surface rises more speedily at $x=2250$ m on the hump, the top part of the wave is raised more up at the $x=3940$ m which is 400 m behind the tip of the third slope of 1/240, and the second short period waves is obviously formed at $x=4740$ m which is 1200 m behind the tip of the

third slope. The first short period wave increases its height while propagating on the mild slopes of 1/240 and 1/100. The maximum height of the wave appears at $x=5946$ m which is 480 m behind the tip of the fourth slope and where the water depth is 17 m approximately, and the wave breaks after it.

RESULTS AND DISCUSSION

To validate STOC-IC with the wave breaking model, calculation results by STOC-IC were compared to the experimental results by Kashima and Hirayama (2013). Each experimental wave flume in Figure 2 was produced in a computation field, which was horizontally divided into square cells whose size Δx ($=\Delta y$) was 5 m constant, and also vertically divided into 15 layers whose minimum height was 3 m. The weighting parameter α for the discretization of the advection terms is set to 0.2.

Figure 5 indicates variations of the maximum water surface elevation (η_{\max}) in space for Case 2 on the bottom with the hump as example, in which d is the water depth, experimental data is indicated by the symbol of a circle as well as results of calculations with and without the wave braking model, and the bottom profile is also illustrated. One of two calculated results with the wave breaking model is of a wave breaking model parameter $\gamma=10$ and the other is of $\gamma=1$. If γ is 10 proposed by Lynett (2006), the calculated wave energy dissipation is weaker than that of the experiment, whereas the calculated result of $\gamma=1$ approaches more the experimental data. Since γ is the parameter to set the transient time of wave breaking, smaller γ likely corresponds to quick energy dissipation such as the plunging breaker. The value of γ , therefore, was set to 1 in the later discussion.

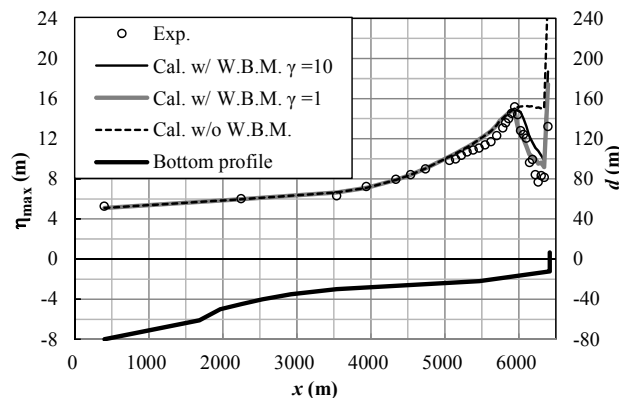
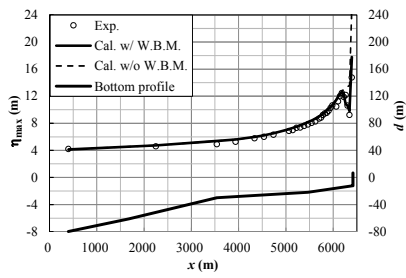


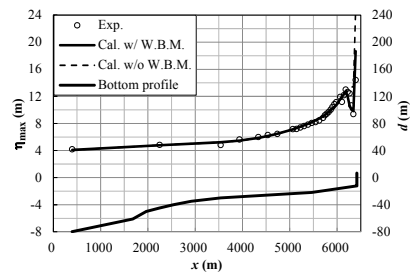
Figure 5. Effect of γ of the wave breaking model in the maximum water surface elevation.

Figure 6 indicates all cases of the spatial variation of the maximum water surface elevation in the same way as Figure 5. The experimental data shows that the solitary waves in all of the cases increase their wave heights on the slope. Based on Green's law derived from wave energy conservation for small amplitude waves, the wave height at the tip of the third slope of 1/240 where the water depth is 30 m is 1.28 times as high as the wave height in front of the wave generator where the water depth is 80 m, and the wave height in front of the breakwater where the water depth is 12.3 m is 1.60 times. On the first slope of 1/67 and the hump where the water depth is deeper than 30 m, the experimental data in all of the cases increase almost in keeping with Green's law, whereas the increase rate on the third and fourth slopes shallower than 30 m is higher than that of the Green's law. In Case 1, Case 2 and Case 5, especially, waves take the maximum heights on the fourth slope of 1/100 and then decrease their heights due to wave breaking.

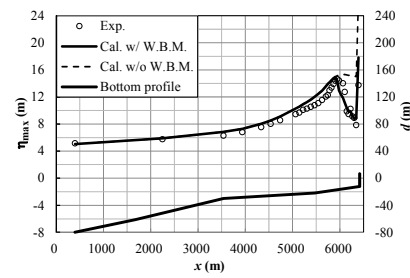
Comparing calculation results and experimental data, the mathematical model of STOC-IC with the wave breaking model well calculates the experimental wave height variations in Case 1, Case 2 and Case 5 which are the wave breaking cases. In these cases, regardless of the hump, the experimental waves take the maximum values at $x=6186$ (720 m behind the tip of the fourth slope and 14.5 m in depth), 5946 m (480 m and 17.0 m in depth), and 6186 m (720 m and 14.5 m on depth), respectively, and then break and decrease their heights. In the numerical simulations the waves take their maximum values at the almost same positions as the experiment. For the no wave breaking cases of Case 3 and Case 4, regardless of the hump, STOC-IC without the wave breaking model is available to be applied to calculation as well as STOC-IC with the wave breaking model.



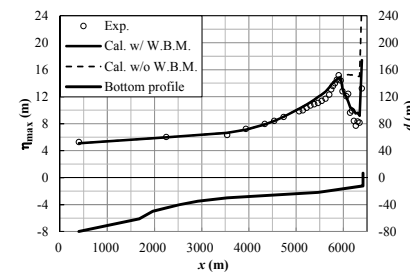
(1) Case 1 on the bottom without a hump



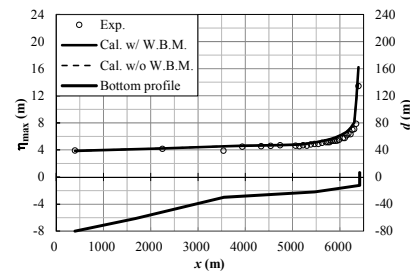
(2) Case 1 on the bottom with a hump



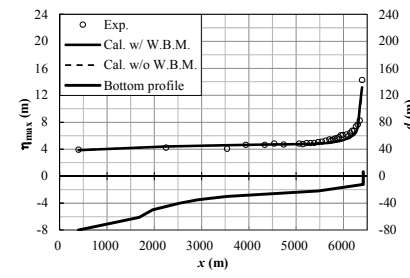
(3) Case 2 on the bottom without a hump



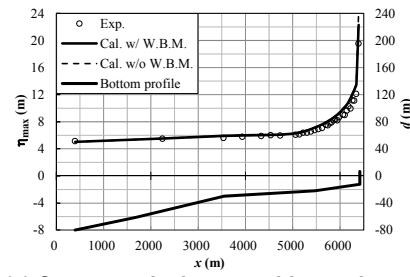
(4) Case 2 on the bottom with a hump



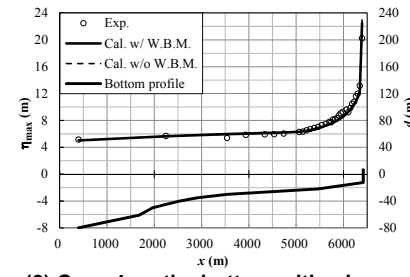
(5) Case 3 on the bottom without a hump



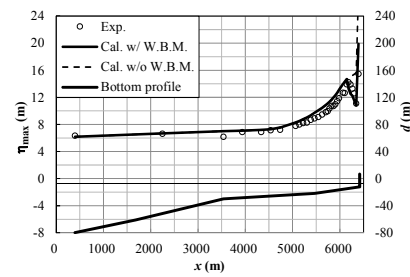
(6) Case 3 on the bottom with a hump



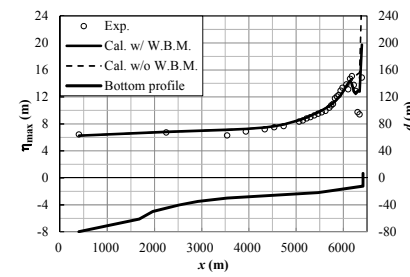
(7) Case 4 on the bottom without a hump



(8) Case 4 on the bottom with a hump



(9) Case 5 on the bottom without a hump



(10) Case 5 on the bottom with a hump

Figure 6. Variations of the maximum water surface elevation in space.

Figure 7 indicates experimental and calculated time waveforms of the water surface elevation in the case of Case 2 on the bottom with the hump in which the experimental wave increased its height remarkably among all of the cases. In figures of (2) and later of Figure 7, a series of the reflected wave from the breakwater appears in the right part of each figure. The waves propagating forward are well calculated by the STOC-IC with the wave breaking model both in the phase and shape of the waveform, comparing with the experimental waveforms: the raised top part of the wave in (2), generation of the short period waves in (3), development of the short period waves in (4) and (5), and the first short period wave decreased by wave breaking in (6). It is, therefore, confirmed that STOC-IC with Kennedy's wave breaking model using Lynett's parameters except for γ is available for calculation of tsunamis accompanied by breaking short period waves. Looking at the reflected waves, there are errors in their phases that should be checked, whereas there are few errors in their shapes.

Figure 8 indicates horizontal velocities at the depth of 8 m below the still water level at $x=5866$ m, 5946 m and 6106 m, corresponding to waveforms of the water surface in (4), (5) and (6) of Figure 7. In the experimental data, the maximum values were not measured at some positions because faster velocities were produced in the experimental flume than the measuring capability of the current meter employed. Therefore, the calculation is not able to be validated in comparison with the experimental data. However, the calculated waveforms are in good agreement with the experimental results except for the shape around the maximum values not measured.

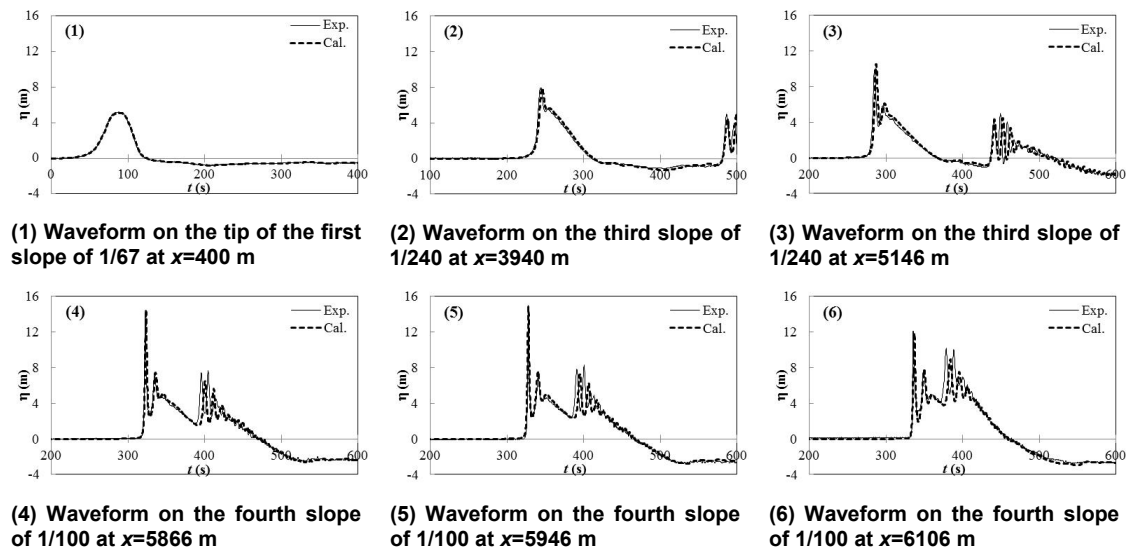


Figure 7. Time waveforms of the water surface elevation in Case 2 on the bottom with the hump.

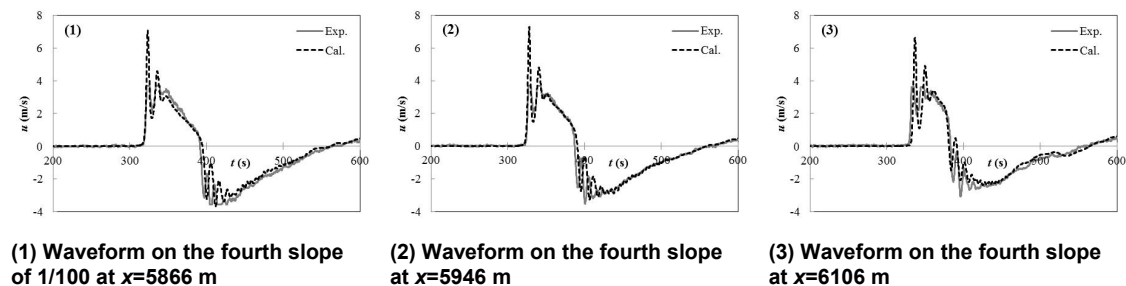


Figure 8. Time waveforms of the horizontal velocity in Case 2 on the bottom with the hump.

CONCLUSIONS

The 2011 Tohoku tsunami in Kuji port was transformed to the undular bore while propagating in the water area of the port, and broken in front of the breakwater installed in the innermost of the port, because the tsunami was very high. For planning and designing measures to save people as well as measures to reduce a tsunami, we need to have any mathematical models to calculate the undular bore and breaking undular bore. In this study, the mathematical model named STOC-IC which was based on

Navier-Stokes equations was applied to calculate the undular bore. Since the original STOC-IC had no wave breaking model, Kennedy's model (Kennedy et al. 2000) was installed in the STOC-IC and Lynett's parameters (Lynett 2006) was applied in the wave breaking model.

Comparing with the experimental data by Kashima and Hirayama (2013) that undular bores with wave breaking and without wave breaking have been generated in the wave flume, the followings were concluded:

1. STOC-IC was able to be applied for calculation of undular bores without wave breaking, because its governing equation was Navier-Stokes equations and therefore no hydrostatic pressure assumption was used.
2. On the parameters in Kennedy's wave breaking model, those proposed by Lynett was able to be applied, except for γ to set the transient time of wave breaking. The parameter γ was set to 1 if Kennedy's wave breaking model was applied to STOC-IC. If γ was set to 10 proposed by Lynett, wave energy dissipation after wave breaking was weaker than that of the experimental data.
3. Calculated results by STOC-IC with the wave breaking model were in good agreement with the experimental data of time waveforms of the water surface elevation.
4. For the horizontal particle velocity, the calculation was not validated around its maximum value because the data was not obtained in the experiment. However, the waveforms of velocity in the experiment were well calculated by STOC-IC with the wave breaking model, except for the profile around the peak velocity.

In the ongoing research works, the developed mathematical model for breaking undular bores is being validated in comparison with pressure in an experiment and inundation caused by the 2011 Tohoku tsunami in Kuji port.

ACKNOWLEDGMENTS

Part of this study was implemented as an activity of the Japan-Chile Joint Research Project named "Enhancement of technology to develop tsunami-resilient community" which is based on the Science and Technology Research Partnership for Sustainable Development (SATREPS) supported by the Japan Science and Technology Agency and Japan International Cooperation Agency. The experimental data was given by Dr. Hiroaki Kashima to validate the numerical model developed in this study. The authors would like to express the deepest appreciation to his kind supplying of the data.

REFERENCES

- Fujima, K., K. Masamura, and C. Goto. 2002. Development of the 2d/3d hybrid model for tsunami numerical simulation. *Coastal Engineering Journal*, 44(4), 373-397.
- Honda, K., and T. Tomita. 2009. Tsunami inundation simulation by three-dimensional model. *Proceedings of 31st International Conference on Coastal Engineering*, ASCE, 1433-1445.
- Ikeno, M., M Matsuyama, T. Sakakiyama, and K. Yanagisawa. 2006. Estimation of tsunami force with breaking of split waves based on model tests, *Report of Central Research Institute of Electric Power Industry*, V05009. (in Japanese)
- Kashima, H., and K. Hirayama. 2013. Model experiments and numerical simulations on tsunami with soliton fission in Kuji harbor, *Journal of JSCE, Ser. B3 (Ocean Engineering)*, 69 (2), I_694-I_699.
- Kennedy, A.B., Q. Chen, J.T. Kirby, and R.A. Dalrymple. 2000. Boussinesq modeling of wave transformation, breaking, and runup. I: 1D, *Journal of Waterway, Port, Coastal, and Ocean Engineering*, 126(1), 39-47.
- Lynett, P.J. 2006. Nearshore wave modeling with high-order Boussinesq-type equations, *Journal of Waterway, Port, Coastal, and Ocean Engineering*, 132(5), 348-357.
- Madsen, P.A., and O.R. Sørensen. 1883. A new form of the Boussinesq equations with improves linear dispersion characteristics, Part 2, A slow-varying bathymetry, *Coastal Engineering*, 18, 183-204.
- Nwogu, O. 1993. An alternative form of the Boussinesq equations for nearshore wave propagation, *Journal of Waterway, Port, Coastal and Ocean Engineering*, 119(6), 618-638.
- PIANC (World Association for Waterborne Transport Infrastructure). 2010. Mitigation of tsunami disasters in ports, Report number 112, 56-61.
- Sakakiyama, T., and R. Kajima. 1992. Numerical simulation of nonlinear wave interacting with permeable breakwaters, *Proceedings of 23rd International Conference on Coastal Engineering*, ASCE, 1517-1530.
- Shuto, N. 2007. Tsunami caused by the Japan Sea earthquake of 1983, *Disasters*, 7(4), 255-258.

Tomita, T., K. Honda, and T. Kakinuma. 2007. Application of three-dimensional tsunami simulator to estimation of tsunami behavior around structures. *Proceedings of 30th International Conference on Coastal Engineering*, ASCE, 1677-1688.